σ-Conjugation and H-Bond-Directed Supramolecular Self-Assembly: Key Features for Efficient Long-Lived Room Temperature Phosphorescent Organic Molecular Crystals

Catherine Demangeat, Yixuan B Dou, Bin Hu, Yann Bretonnière, Chantal Andraud, Anthony d'Aléo, Jeong Weon Wu, Eunkyoung Kim, Tangui Le Bahers, André-jean Attias

σ-Conjugation and H-Bond-Directed Supramolecular Self-Assembly: Key Features for Efficient Long-Lived Room Temperature Phosphorescent Organic Molecular Crystals

Catherine Demangeat, Yixuan Dou, Bin Hu, Yann BretonniHre, Chantal Andraud, Anthony D'Aléo, Jeong Weon Wu, Eunkyoung Kim, Tangui Le Bahers, and André-Jean Attias**

Abstract: Long-lived room temperature phosphorescence from organic molecular crystals attracts great attention. Persistent luminescence depends on the electronic properties of the molecular components, mainly p*-conjugated donor–acceptor (D-A) chromophores, and their molecular packing. Here, a strategy is developed by designing two isomeric molecular phosphors incorporating and combining a bridge for* s*-conjugation between the D and A units and a structure-directing unit for H-bond-directed supramolecular self-assembly. Calculations highlight the critical role played by the two degrees of freedom of the* s*-conjugated bridge on the chromophore optical properties. The molecular crystals exhibit RTP quantum yields up to 20 % and lifetimes up to 520 ms. The crystal structures of the efficient phosphorescent materials establish the existence of an unprecedented well-organization of the emitters into 2D rectangular columnar-like supramolecular structure stabilized by intermolecular H-bonding.*

Introduction

In the field of long-lived room-temperature phosphorescence (RTP) materials, metal-free organic chromophores have attracted in the last decade a growing interest because of their potential applications for example, in organic electronics,[1,2] photonics,[3] information storage,[4] and biotechnologies.[5–7] This was made possible by tackling the intrinsic drawbacks of purely organic materials,[8] that is to say 1) the low intersystem crossing (ISC) rate from the lowest singlet excited state (S_1) to the lowest triplet state (T_1), 2) the rapid rate of non-radiative decay from the triplet state (T_1) to the singlet ground state (S_0), and 3) the quenching of the triplet excitons by interaction with the surrounding oxygen.

Among the different pathways explored to develop metal-free organic materials, the molecular crystal approach is the most studied,[9–20] because addressing simultaneously all the above issues at different length scales. At the molecular level, constitutive individual metal-free organic phosphors mainly consist of *p*-conjugated systems encompassing an emitting subunit. It was demonstrated that the introduction of either heavy halogen atoms or lone-pair electron containing moieties such as carbonyl and sulfonyl groups or heteroatoms enhance the spin-orbit coupling (SOC) and therefore promotes the triplet generation via an efficient ISC process.[13] Within the crystal, it was shown that the intermolecular interactions (H bonds, halogen bonds) and the molecular packing restrain the molecular motions. Thus, minimizing the non-radiative relaxations favors the long-lived spin-forbidden radiative decay from T_1 to S_0. Moreover, the packing mode plays an important role by stabilizing triplet excited states.[14,15] Finally, the dense packing inherent to molecular crystals also prevent, to some extent, the external oxygen quenching by limiting the diffusion. Fulfilling these criteria leads to the realization of metal-free organic crystals exhibiting promising luminescent performances, most often not simultaneously, in terms of phosphorescence efficiency (F_p up to tens of percent),[11,16,17] and phosphorescence lifetime (t_p up to a few seconds).[14,17]

Among all molecular systems investigated for molecular crystals exhibiting long-lived RTP, those integrating carbazole (Cz), one of the archetypical triplet emitter, have been intensively studied, leading to structure-properties guidelines to enhance the performances in terms of ISC and phosphorescence lifetime. Keeping in mind that the ISC is governed by the Fermi's Golden Rule [Eq. (1)] giving the probability to go

$$G_{\delta S_1 @ T_1 P} = \frac{2\pi}{\hbar} \langle T_1 | \hat{H}_{SO} | S_1 \rangle^2 \delta(S_1 - T_1) \quad (1)$$

from the S_1 to the T_1 states, several strategies have been develop based on Equation (1):

[*] Dr. C. Demangeat, Dr. A. D'Aléo, Prof. E. Kim, Dr. T. Le Bahers, Prof. A.-J. Attias
Building Blocks for FUture Electronics Laboratory, UMI 2002, CNRS-Sorbonne Universit8-Yonsei University, Yonsei University
50 Yonsei-ro, Seodaemun-gu, Seoul, 03722 (South Korea)
E-mail: andre-jean.attias@sorbonne-universite.fr
Y. Dou, Prof. B. Hu
Department of Materials Science and Engineering
University of Tennessee
Knoxville, TN 37996 (USA)
Dr. Y. BretonniHre, Dr. C. Andraud, Dr. T. Le Bahers
Univ. Lyon, Ens de Lyon, CNRS UMR 5182, Universit8 Claude Bernard Lyon 1, Laboratoire de Chimie
69342 Lyon (France)
E-mail: tangui.le_bahers@ens-lyon.fr
Prof. J. W. Wu
Department of Physics, Ewha Womans University
Seoul, 03760 (South Korea)
Prof. E. Kim
Department of Chemical and Biomolecular Engineering
Yonsei University
50 Yonsei-ro, Seodaemun-gu, Seoul, 03722 (South Korea)

where $\langle T_1|\hat{H}_{SO}|S_1\rangle$ represents the spin-orbit coupling between the T_1 and S_1 states and $1/(S_1 - T_1)$ is the overlap of the S_1 and T_1 density of states, enhanced when the energy gap between these two states (called after ΔE_{ST}) is the smallest.

One strategy for achieving long-lived RTP in molecular crystals from carbazole-based molecules is to couple moieties with different angular momentum singlet and triplet excited states to satisfy the El Sayed's selection rule (originated from the $\langle T_1|\hat{H}_{SO}|S_1\rangle$ term). This can be done by linking a n-unit (n–π^* transition) to a carbazole π-unit (π–π^* transition). It was demonstrated that this design, besides an intramolecular coupling, can lead also, within the crystal, to an intermolecular electronic coupling that favors the ISC from the n-unit to the π-unit, enhanced after the introduction of a heavy halogen atom.[18]

Another design strategy consists in coupling the carbazole electron-donating (D) group to an electron-accepting (A) group into a twisted (D-A) system to favor a twisted intramolecular charge-transfer (TICT),[19,20] one of the ways to generate triplet states via charge transfer states.[21] Indeed, such a twisted structure is well known in the field of molecules exhibiting thermally activated delayed fluorescence (TADF) for promoting a spatial separation of the highest occupied molecular orbital (HOMO) and the lowest unoccupied molecular orbital (LUMO), that leads to a small ΔE_{ST} and an increase of the ISC rate.[22] Ultimately, by controlling the intramolecular energy transfer between triplet excited states of the D and A groups and introducing a heavy atom such as bromine, the twisted phosphors approach allows to reach phosphorescence quantum yield and lifetime up to 41 % and 0.54 s, respectively.[16]

Apart the above engineering rules at the molecular level, the molecular packing into carbazole-based crystals also plays a crucial role to understand the long-lived phosphorescence. In particular, H-aggregates observed in dimeric structures of planar carbazole-based chromophores can lead to long excited state lifetimes (> 1 s) by stabilization of the triplet excited states (phosphorescence quantum yield up to 1.25 %).[14] On the other hand, it was also demonstrated that the more compact face-to-face packing of carbazoles leads to a long lifetime (750 ms) attributed as well to the stabilization of the excited triplet state, with an efficiency of&3 %.[12] Nevertheless, the arrangement of carbazoles as a herringbone motif without π-to-π coplanar interaction is also emphasized to contribute to the aggregation effect.[20]

Despite carbazole-based long-lived phosphorescent crystals have been obtained, there are challenges that need to be addressed at the different scales in view of a better understanding of the structure-properties relationships. At the molecular level, the important issue deals with the ISC efficiency, since in most of the above results the emission is dominated by fluorescence process. However, the management of the ISC rate is not an easy task since it is dominated by the SOC that appears to be a dynamical phenomenon strongly affected by the distortion of the molecule more than an intrinsic property of the molecule, as recently demonstrated.[23–25] In those works, it was shown that molecules having some degrees of freedom (generally rotations between two fragments) are more prone to find a configuration leading to a strong SOC. The second challenge deals with the carbazole-based crystals structure. It aims to identify the common structural feature whose optical fingerprint is the yellow RTP generally observed in reported literature and leading to similar emission spectra with a vibronic structure. This should allow to steer the assembly of specifically designed phosphors into this crystal architecture.

In this context, the rational design of molecular emitters with controlled topology and electronic properties on the one hand, and capable to form well-defined supramolecular self-assemblies where molecular ordering determines the materials properties on the other hand, is particularly appealing. With this aim, hydrogen bonds are particularly attractive to direct the self-assembly as they are directional and can be easily introduced by equipping the molecular phosphor with an adapted supramolecular recognition element (synthon) acting as structure-directing functional group.

Here, we propose a novel strategy hinging on hydrogen-bond-directed supramolecular self-assembly of a new class of D-A carbazole-based phosphors (Scheme 1). Compared to common RTP organic materials, the novelty of the design concept consists in σ-conjugation[26,27] (instead of π-conjugation more frequently found) between the D and A moieties and the use of pyridine as simultaneously n-type and A unit as well as synthon for supramolecular self-assembly. More precisely, we designed and synthesized two regioisomers of a new family of carbazole-based chromophores where the (D) Cz unit and the (A) pyridine ring are connected via a bridge consisting of a triple bond linked to a sp^3-C (-CH_2- group). This unusual spacer was chosen to allow rotations around the two single bonds (Scheme 1 a) and to investigate the influence of the conformation induced by these two degrees of freedom on 1) the singlet-triplet energy gap (ΔE_{ST}) and 2) the efficiency of the SOC. We also aimed at enhancing the formation of triplet excited state taking advantage of the hyperconjugation.[28] With this aim, intensive (TD-)DFT calculations were performed and the systematic simulation of molecular spectroscopic properties as a function of the two degrees of freedom allows to draw properties maps giving the atomistic interpretation of the optical properties. These calculations rationalize the completely different spectroscopic behavior in dilute solution and in crystalline state. On the other hand, whatever the position on the pyridine ring of the nitrogen atom and of the bromine atom introduced to favor ISC, in the solid state the two isomers (T2-p-PyCzBr and T3-m-PyCzBr)

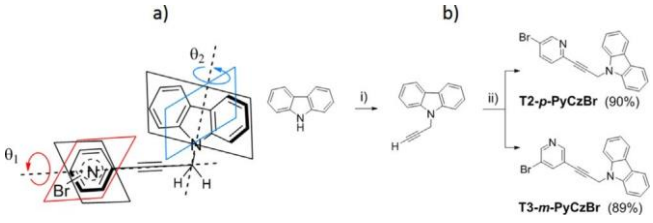

Scheme 1. a) General molecular structure of the target compounds with the corresponding dihedral angles q_1 and q_2. b) Synthesis of T2-p-PyCzBr and T3-m-PyCzBr derivatives: i) KOH, Propargyl bromide, DMF, 0&C to RT, 6 h; ii) $Pd(PPh_3)_2Cl_2$, CuI, Et_3N, 3-bromo-2-iodopyridine or 3-bromo-5-iodopyridine RT, 12 h.

with the same conformation exhibit roughly identical emitting properties almost completely dominated by efficient long-lived yellow phosphorescence with both high phosphorescent quantum yield (up to 20 %) and long lifetimes (up to 524 ms). Moreover, a deep single crystal analysis reveals an unprecedented well-organized 2D rectangular columnar-like supramolecular structure stabilized by intermolecular H-bonding. Overall, our strategy based on the rational design of metal-free organic chromophores for supramolecular self-assembly and our findings open new perspectives for the realization of organic molecular crystals exhibiting long-lived RTP.

Results

The two regioisomers T2-*p*-PyCzBr and T3-*m*-PyCzBr were easily synthesized through a two-step procedure (Scheme 1 b). First, carbazole was linked to the propargyl bromide, and a subsequent Sonogashira cross coupling of the resulting acetylenic precursor with the corresponding 3-bromo-2-iodopyridine and 3-bromo-5-iodopyridine afforded the target compounds with high yields of ca. 90 % (for details see the Supporting Information). They were fully characterized by ^{1}H and ^{13}C NMR, and mass analysis (Supporting Information). Single-crystals for X-ray diffraction (XRD) were grown by slow evaporation from a mixture of n-hexane and methylene chloride at room temperature. Three crystals, comprising two polymorphs, were obtained and characterized by thermal analysis and XRD (Supporting Information).

Time-dependent density-functional theory (TD-DFT) calculations were used to investigate the molecular spectroscopic properties of T3-*m*-PyCzBr as a function of the two dihedral angles q_1 and q_2 (Scheme 1; Supporting Information, Scheme S1 and Figure S1a) with the aim to determine the influence of these two main degrees of freedom (via the methylene spacer) on the ground and excited states properties. The geometries of three electronic states were relaxed corresponding to the ground state (S_0) and the first singlet excited states (noted $^{1}LE_C$ and $^{1}CT_{cp}$). All properties were computed using the range separated hybrid functional cam-B3LYP, a double-zeta all electron basis set and CH_2Cl_2 as implicit solvent. All computational details are given in supporting information (Supporting Information).

The ground state potential energy surface (Supporting Information, Figure S1b) shows that the rotations around the triple bound (q_1) and of the carbazole (q_2) are below 10 kJmol$^{@1}$ and 20 kJmol$^{@1}$, respectively. Thus, the molecule can scan all the possible values of these angles in the ground state at room temperature. Figure 1a depicts the Jablonski diagram obtained by using the transition energies computed for the most stable geometry of each of the three potentials energy surfaces considered. This diagram indicates that the two first singlet excited states are localized on the carbazole (both noted $^{1}LE_c$) while the third singlet excited state is a charge transfer state between the carbazole and the pyridine moiety (noted $^{1}CT_{cp}$).

Interestingly, when relaxing the geometry at the excited state, the molecule first stays in the first $^{1}LE_c$ state with a geometry almost similar to the one in the ground state

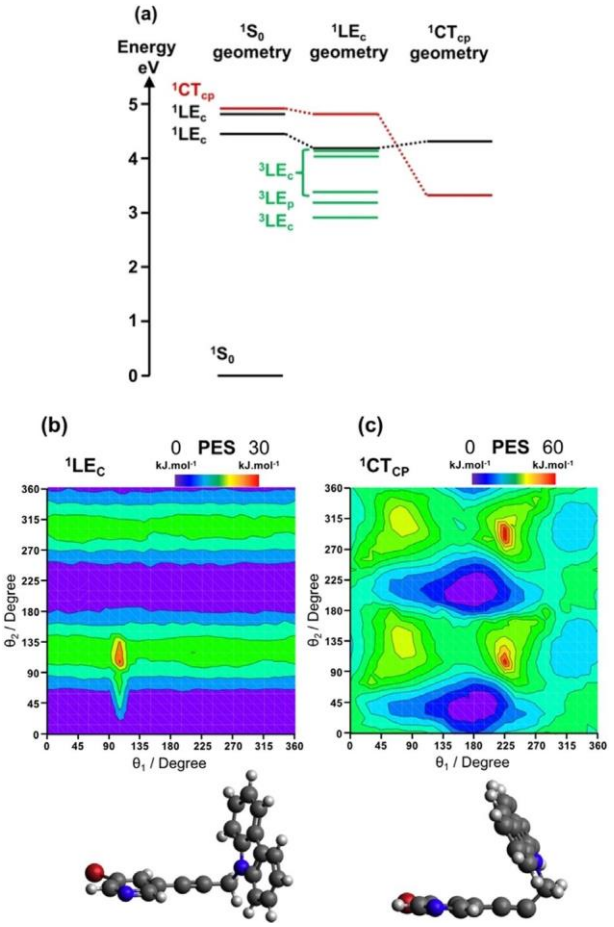

Figure 1. a) Jablonski diagram of T3-*m*-PyCzBr. b),c) Potential energy surfaces (PES) associated to the $^{1}LE_c$ (b) and $^{1}CT_{cp}$ states (c). The structures below each map correspond to the most stable conformation of each map. (coordinates of these structures are given in Supporting Information, Tables S1–S3).

(middle of the Jablonski diagram on Figure 1 a). But a slight loss of linearity of the triple bond associated to a small energy barrier (ca. 0.15 eV) induces an important reorganization of the excited states leading to the $^{1}CT_{cp}$ state as the most stable excited state (right side of the Jablonski diagram Figure 1 a) in CH_2Cl_2 as PCM solvent. The potential energy surfaces (PES) associated to the $^{1}LE_c$ and $^{1}CT_{cp}$ states and a drawing of the geometries of the molecule at the most stable configuration for each PES are given in Figure 1 b.

The fluorescence emission wavelength from the $^{1}LE_c$ state ($\lambda_{emi}{}^{1LEc}$) is computed around 296 nm with an oscillator strength f^{1LEc} around 0.15 whatever the two angles considered confirming the localized nature of the transition. On the contrary, the characteristics of the fluorescence emission from the $^{1}CT_{cp}$ state are extremely sensitive to the conformations (Figure 2). As shown on Figure 2 a, the fluorescence emission wavelength from the $^{1}CT_{cp}$ state ($\lambda_{emi}{}^{1CTcp}$) ranges from 310 to 420 nm. Very interestingly, the oscillator strength of the emission (f^{1CTcp}) can vary from almost 0 (forbidden transition) to almost 0.25 (allowed transition) for very specific combination of angles (Figure 2 b). The large oscillator strength computed for some angles is due to the mixing between the

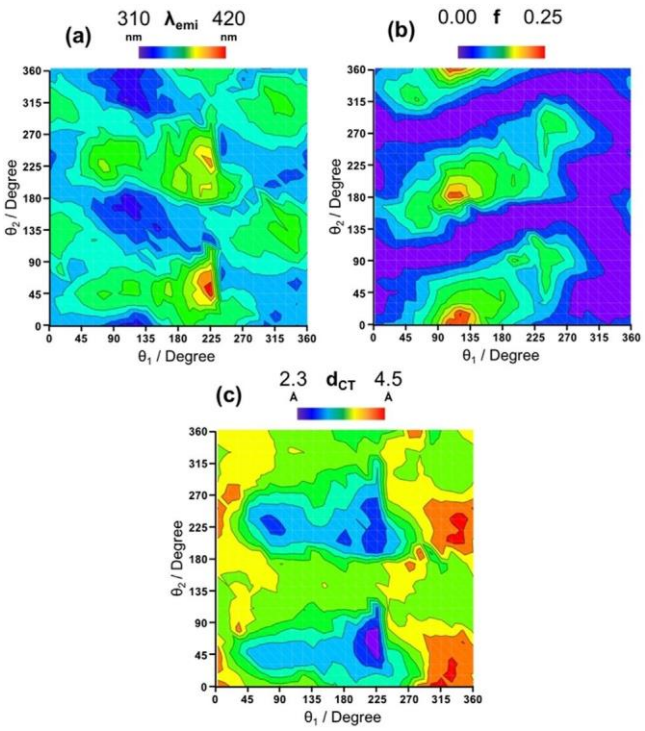

Figure 2. Properties of the $^1CT_{cp}$ state including a) the wavelength emission, b) the oscillator strength, and c) the charge transfer index associated to this state.

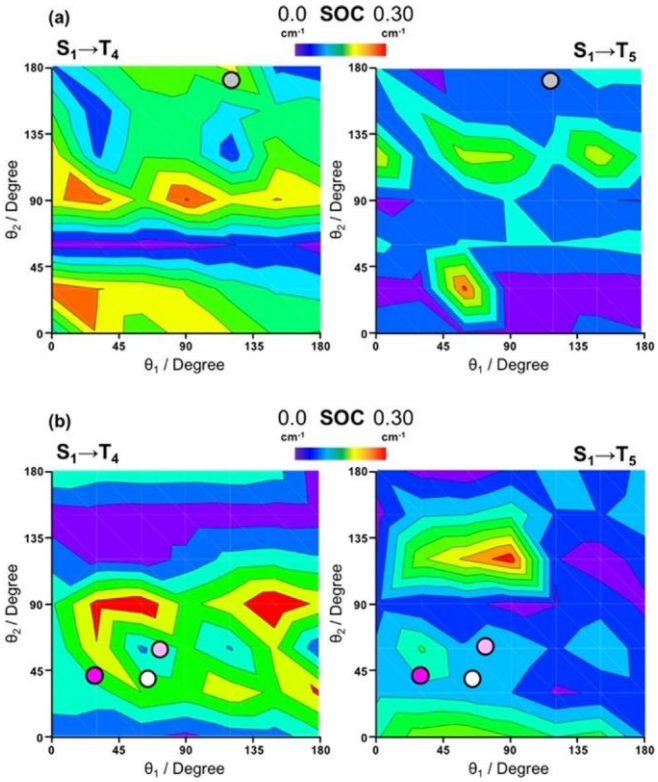

Figure 3. Computed SOCs between T_4 and ^1LE_c and T_5 and ^1LE_c for both T3-*m*-PyCzBr (a) and T2-*p*-PyCzBr (b) as a function of the angles q_1 and q_2. The grey, white, pink, light pink circles correspond to the position of T3-*m*-PyCzBr, T2-*p*-PyCzBr-C1, T2-*p*-PyCzBr-C2-a and T2-*p*-PyCzBr-C2-b using angles extracted from XRD refinement, respectively. Values computed at the cam-B3LYP/cc-pVDZ-DK/CH_2Cl_2 PCM level.

$^1CT_{cp}$ state and a higher energy excited state, localized in nature and having a large oscillator strength. This is quantified by the d_{CT} charge transfer index,[29,30] quantifying the length of a charge transfer transition (Figure 2 c). The zone for which the oscillator strength is large (>0.1) corresponds both to the smallest values of d_{CT} and to the most stable area of PES (Figure 1 b). It is extremely interesting to see that the methylene group introduced to decouple the D unit from the A unit does not extinct completely the emission CT band. It is also very important to note that the possibility to couple with higher excited state is necessary to explain the strong emission from the $^1CT_{cp}$ state.[31]

The possibility to populate triplet excited states was also considered. The reference state is the ^1LE_c state since we assume that the distortion necessary to stabilize the $^1CT_{cp}$ state is not possible in solid state. TD-DFT calculations were performed on the optimized ^1LE_c geometry to determine the nature of the triplet excited states accessible from the ^1LE_c state and the SOC between these states. As shown in the Jablonski diagram (Figure 1 a, middle of the diagram), five triplet excited states were computed below the ^1LE_c (four localized on the carbazole and one localized on the pyridine). The range of values of the DE_{ST} and of the SOC are given in the Supporting Information, Table S1. Since the T_5 state is extremely close in energy to the ^1LE_c state ($DE_{ST} = 0.03$–0.09 eV), the ISC between these two excited states can be promoted. The SOC map between T_5 and ^1LE_c (Figure 3) shows that the strength of the SOC is sensitive to the conformation of the molecule (q_1 and q_2), ranging from 0.02 to 0.36 cm^{-1}. Thus, it can be inferred that the conformation of the molecule in the solid state will have strong influence on the final ISC and on the phosphorescence efficiency of molecular crystals, as we will see in the following. The SOC maps for the four remaining triplet states are reported in Figure 3 and in the Supporting Information, Figure S2 and S3.

UV/Vis electronic absorption and emission spectra of the two compounds T3-*m*-PyCzBr and T2-*p*-PyCzBr in methyl- ene chloride dilute solution (DCM, 10^{-6} M) at room temper- ature are reported on Figure 4a and b, respectively. Whatever the isomer, the absorption spectra are similar with an intense peak at 292 nm (generally associated to the ^1L_a ← 1A (p-p^*) transition of Cz), and two weak absorption peaks at 325 and 338 nm (also associated to the ^1L_b ← 1A (n-p^*) transition of Cz),[32,33] in good agreement with the computed first transitions localized on the carbazole unit. The CT absorption band is not observed since computed higher in energy than the localized excited state transitions (around 5.0 eV compared to 4.4 eV and 4.8 eV for the two LE transitions) on the one hand, and weaker in intensity (around 0.05 a.u. for the oscillator strength compared to 0.1 a.u. and 0.5 a.u. for the two LE transitions) on the other hand. Its overlap with the LE bands could explain why it is not possible to observe the CT band.

The steady state fluorescence spectra (excitation at 310 nm) of both isomers show a dual-emission exhibiting an identical feature. It consists in structured transition composed of two well-resolved sharp bands at 342 and 353 nm ascribed

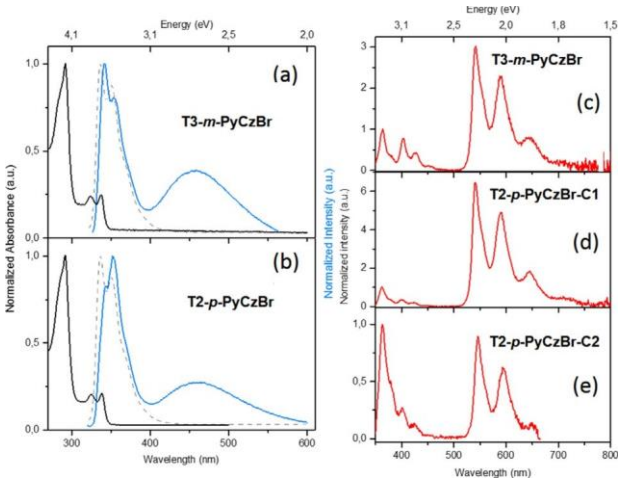

Figure 4. Photophysical properties. a),b) Normalized absorbance (plain black line) and emission (excited at 310 nm, plain blue line) spectra of a) T3-*m*-PyCzBr and b) T2-*p*-PyCzBr in DCM ($10^{@6}$ M); emission of a carbazole solution (dashed grey line) in the same conditions. c)–e) Emission spectra in the crystalline state (excitation at 340 nm) of c) T3-*m*-PyCzBr, d) T2-*p*-PyCzBr-C1, and e) T2-*p*-PyCzBr-C2.

to the emission of the carbazole moiety with LE character and a broad structureless band at around 465 nm, red-shifted as the solvent polarity increases indicating the charge-transfer (CT) character of this band. This observation confirms the existence of two possible stable excited electronic structures, called ^1LE_c and $^1CT_{cp}$ in the previous section. Even if the $^1CT_{cp}$ excited state is notably more stable than the ^1LE_c excited state after relaxation, the barrier required to go from one excited state to another allows keeping a part of the molecules in the ^1LE_c state leading to a dual fluorescence spectra. Since this dual fluorescence is seen for both molecules, we can reasonably postulate that the mechanism of the dual fluorescence is the same for the two molecules.

At 77 K, in a deaerated dilute solution of ethanol/methanol (80:20), when excited with a UV lamp (365 nm), T2-*p*-PyCzBr and T3-*m*-PyCzBr display a long-lived blue luminescence that last few seconds after the excitation is switched off. This qualitative behavior shows that at the monomeric level, the molecules are able to exhibit phosphorescence as long as the molecular motions were suppressed. A deeper quantitative analysis shows that the emission spectra of both isomers measured at 77 K (Supporting Information, Figure S4a,b) are similar, consisting of a main structured peak (340–375 nm) and a broader structureless band (415–525 nm) attributed to fluorescence and phosphorescence, respectively. This is confirmed by time-gated experiments in which the higher energy peak disappears while the broader peak remains visible. Note that the wavelength range (450 nm) and shape for the latter resemble those of a frozen solution of carbazole,[34] demonstrating that the low temperature phosphorescence arises from the isolated carbazole moiety.

All the above results indicate that both isomers have the same photophysical properties in dilute solution.

However, in the crystalline state, photophysical properties (nature of the emission, photoluminescence quantum yields, and lifetimes) of T2-*p*-PyCzBr and T3-*m*-PyCzBr strongly depend on the isomerism and polymorphism. At room temperature, both T3-*m*-PyCzBr and a polymorph obtained for T2-*p*-PyCzBr (namely, T2-*p*-PyCzBr-C1) irradiated with UV lamp (λ_{ex} = 365 nm) exhibit intense yellow afterglow which lasts over 4 seconds after the removal of the excitation light. On the contrary, polymorph T2-*p*-PyCzBr-C2 displays a weaker orange emission which faints much more quickly (ca. 1 s) after turning off the UV lamp.

Figure 4 c–e presents the photoluminescence (PL) spectra of the three single crystals of T3-*m*-PyCzBr, T2-*p*-PyCzBr-C1, and T2-*p*-PyCzBr-C2 under ambient conditions (at 300 K, in air), respectively. Decay profiles are presented on Figure S5 and the excited state lifetimes are reported in Table S5. T3-*m*-PyCzBr and T2-*p*-PyCzBr-C1 exhibit identical steady-state spectra (Figure 4 c,d, respectively) with weak emission bands in the 370 to 450 nm wavelength region and intense emission peaks at 540, 589 and 640 nm with a vibronic progression (0.18–0.19 eV). Since the photophysical behavior in crystal and in dilute solution at 77 K are different, we can infer that the emission does not originate from the same species. It is worth noting that the broad emission band observed in solution and associated to the charge transfer transition has disappeared in the solid state. As we have discussed earlier, the population of the CT state is only possible if an important distortion of the molecule is accessible (the loss of linearity of the triple bound) that is possible in solution but probably not when the molecule is in the solid state explaining the disappearance of this emission. As shown in the Supporting Information, Figure S5a,b and Table S5, the excited state lifetimes values of the high energy emission for T3-*m*-PyCzBr and T2-*p*-PyCzBr-C1 are 0.45 and 0.77 ns (at 365 and 363 nm, respectively), clearly indicating the fluorescence nature of the emission with the corresponding fluorescence quantum yield (Φ_{Fl}) of 2.0 and 1.5 %. Regarding the lower energy emission, the excited state lifetimes values of T3-*m*-PyCzBr and T2-*p*-PyCzBr-C1 were found to be as high as 524 and 432 ms (at 542 and 543 nm) (Supporting Information, Figure S5d,e), with the related phosphorescence quantum yield (Φ_{Ph}) of 9.0 and 20.0 %, respectively, demonstrating an outstanding long-lived RTP. On the contrary, the steady-state emission spectrum of T2-*p*-PyCzBr-C2 (Figure 4 e) reveals that the fluorescent emission between 370 to 450 nm is stronger, whereas the low-energy phosphorescence emission (540, 589 and 640 nm) is much weaker together with a drastic decrease of the lifetime (42 ms; Supporting Information, Figure S5f and Table S5).

To better understand the relationship between the solid-state photoluminescent properties and the molecular packing, single-crystal X-ray diffraction analysis of T3-*m*-PyCzBr and of the two polymorphs T2-*p*-PyCzBr-C1 and T2-*p*-PyCzBr-C2 was carried-out (Supporting Information, Table S7–S9). Bond lengths and angles of interest are reported in the Supporting Information, Tables S10, S11, and S12 for T3-*m*-PyCzBr, T2-*p*-PyCzBr-C1, and T2-*p*-PyCzBr-C2, respectively. The stacking parameters are reported in Table S13.

T2-*p*-PyCzBr-C1 crystallizes in the monoclinic *C*2/*c* space group with eight (Z = 8) independent molecules per unit cell (Supporting Information, Table S8). In the crystal, the molecule adopts a nearly perpendicular conformation be-

tween the carbazole long axis and the pyridine ring with θ_1 = 66.5° and θ_2 = 38.7° (ca. 6° and 7° deviation from orthogonality, respectively), whereas the ethynylene linkage is slightly bent (10.33°; Figure 5b; Supporting Information, Scheme S1).

Moreover, the carbazole and pyridine dipole moment vectors point in the same direction. In the unit cell, the basic structure consists of the arrangement of the eight T2-*p*-PyCzBr-C1 molecules into four parallel pairs with the carbazole long axis in planes perpendicular to the *b* axis whereas the sp^2 lone pair orbitals of the nitrogen atoms are directed along the *b* axis (for a more detailed description see the Supporting Information and Figure S6). At a larger scale, the repetition of the unit cell through regular translations along the three *a*, *b*, and *c* axis leads to an unprecedented well-organized 2D rectangular columnar-like supramolecular structure stabilized by intermolecular H-bonding, with two remarkable main features as depicted on Figure 6a and sketched on Scheme 2. First, pyridine rings self-assemble in supramolecular linear chains through hydrogen bonding along the *b* axis (N···H@C = 2.31 Å) and are translated by a unit cell length (6.03 Å) along this direction. This drives the stacking along the *b* axis of the directly connected carbazole units, with an interplanar distance $d_{interpl}$ = 2.73 Å. Second, the self-assembly of the carbazole units form two slipped stacks along the *b* axis, each alternate stacks translated by a unit cell length along the stack direction, leading to the formation of a column. The carbazole units are both tilted by θ = 27.34° in opposite directions with respect the *b* axis (herringbone motif), with the Cz permanent dipole moment projection along *b* axis pointing in the same direction (repulsive interaction). Further, the carbazole molecular columns self-assemble to give a two-dimensional (2D) rectangular columnar arrangement (a_{colr} = 13.92 Å and b_{colr} = 9.46 Å). It is worth noting that the dipole moments projection of the carbazole units along the *b* axis point in the same direction (up or down) into a given column (Supporting Information, Table S13) and have the same orientation in the columns along the short a_{colr} whereas the orientations alternate (up and down) along long axis b_{colr} (Figure 6a).

In comparison, T3-*m*-PyCzBr crystallizes in the monoclinic *P*21/*n* space group with four independent molecules

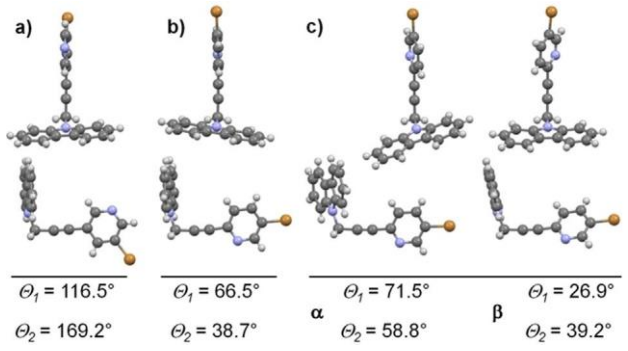

Figure 5. Molecular conformation in the single crystals of a) T3-*m*-PyCzBr, b) T2-*p*-PyCzBr-C1, and c) T2-*p*-PyCzBr-C2 (conformers a and b).

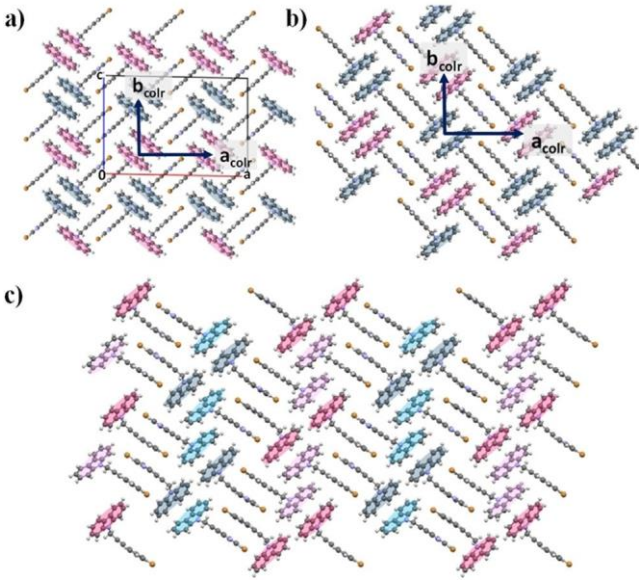

Figure 6. Packing diagram for single crystals of a) T2-*p*-PyCzBr-C1, b) T3-*m*-PyCzBr, and c) T2-*p*-PyCzBr-C2, viewed along the *b* axis. Carbazole units with dipole moment up and down are highlighted in red and blue, respectively. For T2-*p*-PyCzBr-C2 carbazole unit of *a* and *b* conformers with dipole moment up (down) are highlighted in light and dark red (light and dark blue), respectively. a_{colr} and b_{colr} are the axis of the supramolecular 2D rectangular network of columns of carbazole units.

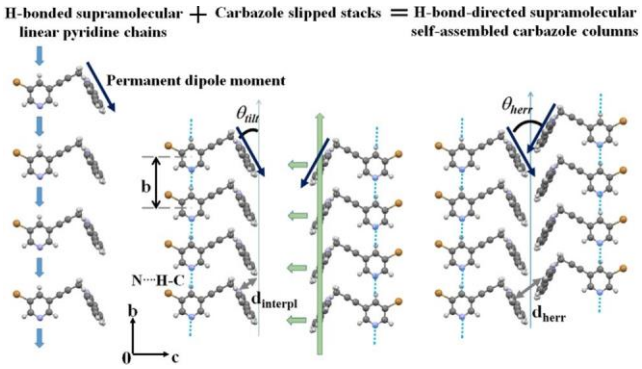

Scheme 2. How the H-bonded supramolecular linear pyridine chains drive the formation of carbazole slipped stacks leading to the obtention of H-bond-directed supramolecular self-assembled carbazole columns. The parameters of the stacking for T3-*m*-PyCzBr, T2-*p*-PyCzBr-C1, and T2-*p*-PyCzBr-C2 are reported in the Supporting Information, Table S13.

(*Z* = 4) per unit cell (Supporting Information, Table S7) and adopts in the crystal roughly the same nearly perpendicular conformation as T2-*p*-PyCzBr-C1 (θ_1 = 116.5° and θ_2 = 169.2°), with a slightly less bent ethynylene linkage (6.22°) (Figure 5 a). On the other hand, the carbazole and pyridine dipole moment vectors points in up and down opposite directions, respectively. Interestingly, despite in the unit cell the molecules are organized in two pairs (Supporting Information, Figure S7), the supramolecular self-assembly of the T3-*m*-PyCzBr molecules leads to a crystal structure exhibiting the same features as T2-*p*-PyCzBr-C1, as depicted

on Figure 6b (for a more detailed description, see the Supporting Information and Table S13). Here, the dipole moments projection of the carbazole units along the *b* axis point in opposite directions into the four first neighbor columns.

Interestingly, for T2-*p*-PyCzBr-C2, that crystallizes in the monoclinic *P*21/*n* space group with eight independent molecules (*Z* = 8) per unit cell (Supporting Information, Table S9), the constitutive molecules adopt two different conformations *a* and *b* with the associated twist angles (θ_1 = 71.58 and θ_2 = 58.88) and (θ_1 = 26.98 and θ_2 = 39.28), respectively (Figure 5 c). Thus, the *a* and *b* conformations deviate from the nearly perpendicular one at the level of the orientation of either the carbazole unit or the pyridine ring, respectively. In the unit cell, the molecular packing exhibits two unexpected main features (Supporting Information, Figure S8). First, whatever the conformation, the pyridine units planes are parallel with the sp^2 lone pair orbital of the nitrogen atom directed along the *b* axis like for T3-*m*-PyCzBr and T2-*p*-PyCzBr-C1. Second, compared to T2-*p*-PyCzBr-C1, a subtle interplay between the *a* and *b* conformations leads to the formation of head (Cz from *a* conformer) to head (Cz from *b* conformer) pairs. Surprisingly, as for T2-*p*-PyCzBr-C1 and T3-*m*-PyCzBr crystals, the pyridine rings in the crystal are translated by a unit cell length (6.02 c) along the stack direction *b* and self-assemble via hydrogen bonding along the same direction, with N···H-C = 2.31 and 2.35 c for stacks from *a* and *b* conformations, respectively (Supporting Information, Table S13). Thus, carbazoles units form two distinct slipped stacks that built a carbazole column, where the carbazole interplanar distance are 3.21 and 3.12 c for units from the *a* and *b* conformations, respectively. Now, pairs of two adjacent columns with partial overlap of carbazoles form are considered to describe the 2D network, as depicted on Figure 6 c.

It is obvious that whatever the crystal, there is no H aggregation and the organization of the carbazole units within the herringbone columns is the common thread.

Discussion

Combining single crystal analysis and photophysical behavior allows establishing some structure-properties relationships and highlighting key features for efficient long-lived room temperature phosphorescence of organic molecular crystals. The very low fluorescence associated to an intense phosphorescence for T3-*m*-PyCzBr and T2-*p*-PyCzBr-C1 crystals results from an efficient singlet exciton nonradiative decay way that simultaneously populates a triplet excited state from which subsequent internal conversion (IC) leads to the phosphorescent state. This efficient intersystem crossing (ISC) from the singlet to the triplet excited states is allowed by enhanced spin-orbit coupling (SOC) attributed to the heavy atom effect induced by the introduction of the bromine atom on the pyridine ring. Here, the heavy atom effect could originate from an intra and an intermolecular contribution to the SOC. The internal contribution is deduced from the TD-DFT modeling based on the SOC map presented in Figure 3 where the coordinate of the T3-*m*-PyCzBr molecule in the solid (θ_1 = 116.58 and θ_2 = 169.28) is reported. Taking into consideration the coupling of S_1 with T_5 and T_4 because of their close energies (Figure 1; Supporting Information, Table S4) a summed of around 0.39 $cm^{@1}$ is obtained. Thus, both this significant SOC and the small ΔE_{ST} and finally a large ISC rate explain the high phosphorescence efficiency. On the other hand, the crystalline structure (Supporting Information, Figure S9 and Table S13) shows that the Br atom is located close to the carbazole unit with a Br–Cz distance of ca. 3.36 c, allowing a possible intermolecular heavy atom effect.[35] A similar situation is found for T2-*p*-PyCzBr-C1 giving the same conclusion. Since T2-*p*-PyCzBr-C2 crystal exhibits both fluorescence and phosphorescence, it is possible to discriminate the precise role of the intra and intermolecular contribution of the heavy atom effect. As shown by the modeling, the molecule in the *a* conformation (θ_1 = 26.98 and θ_2 = 39.28) has a SOC value similar to that computed for the T3-*m*-PyCzBr crystal (around 0.33 $cm^{@1}$). In contrast, there is a drastic decrease of the SOC (0.13 $cm^{@1}$) for the *b* conformation (θ_1 = 71.58 and θ_2 = 58.88), that finally leads to a less efficient SOC. Because in the meantime the intermolecular Br–carbazole distances in the crystal remain unchanged, it is inferred that the less efficient ISC can thus be attributed mainly to the decrease of the intramolecular heavy atom effect. These results demonstrate that in our molecular crystals the ISC is dominated by the intramolecular SOC component.

The orientation of the permanent dipole moment of the carbazole units within a column could explain the observation of not the blue phosphorescent emission from the monomeric carbazole but the yellow one, with vibronic peaks at 540, 589, and 640 nm. In the pure crystalline carbazole, this emission is weak and originates from the triplet excited state of a dimer or carbazole pair.[34,36] In the carbazole crystal, the molecules stacks along the *c* axis to also form columns consisting of two slipped-stacks that are both tilted by 28° in opposite directions with respect to this axis and translated by half a unit cell (2.84 c) along the stack direction (herringbone structure) (Figure S10). However, compared to T3-*m*-PyCzBr and T2-*p*-PyCzBr-C1 and -C2, the permanent dipoles moments point in opposite directions. Thus, we can infer that the dimer or carbazole pair is the herringbone motif where Cz units have the same orientation. In the crystal of pure carbazole, it occurs only when there is a defect in the structure, which could explain the weak phosphorescent emission. In T3-*m*-PyCzBr and T2-*p*-PyCzBr, the H-bond-directed self-assembly of the pyridine cores force the same orientation of the Cz units leading exclusively to the yellow emission. It is worth noting that the interaction between two adjacent Cz units, repulsive in the ground state (dipole moment pointing in the same direction), becomes attractive between an excited unit and its unexcited neighbor thanks to the inversion of the dipole moment in the excited state.[37]

Finally, T3-*m*-PyCzBr and T2-*p*-PyCzBr-C1 have phosphorescence lifetime of the same order of magnitude, that is, several hundreds of ms, whereas for T2-*p*-PyCzBr-C2 it is only a few tens of ms. The packing of the carbazole units in these molecular crystals could explain these differences.

Exciton diffusion plays more broadly a pivotal role in organic electronics, where the diffusion occurs in a conjugated material through Dexter-type energy transfer.[38–40] This short distance process proceeds by hopping and requires good overlap of molecular orbitals to ensure the double electron transfer, from the HOMO and LUMO of two neighboring molecules. In T3-*m*-PyCzBr and T2-*p*-PyCzBr-C1, the triplet excitons can only diffuse in its own column; it cannot hop to the neighbor column because of the inversion of the carbazole short axis orientation between two adjacent columns and their very small overlap. Because of the long distance (ca. 6 c) between parallel molecules in a column, the transfer should occur via zig-zag diffusion along the herringbone structure. This process could lead to a short triplet diffusion distance, which prevents to reach nonradiative traps and leads to a long-lived phosphorescence as for T3-*m*-PyCzBr and T2-*p*-PyCzBr-C1. The lifetimes are similar for both crystals because the same crystal structure should lead to the same pathway for triplet exciton diffusion on the one hand, and similar nonradiative rates for intramolecular vibrational relaxation and triple quenching by the surrounding on the other hand. In T2-*p*-PyCzBr-C2 crystal, the triplet exciton could hop to the neighbor column of the column pair because of the partial overlap of Cz units with the same permanent dipole orientation in two adjacent columns. Thus, triplet diffusion distance increases along with opportunities to find a trap, which could explain the shorter lifetime.

Conclusion

Based on the rational design of metal-free chromophores capable of H-bonded directed supramolecular self-assembly and s-conjugation, we provide a new approach to obtain molecular crystals exhibiting outstanding long-lived room temperature phosphorescence (F_{Ph} and t_{Ph} up to 20 % and 520 ms, respectively). According to this strategy, we synthesized two regioisomers of a new chromophores family where a carbazole unit and a pyridine ring are connected via a bridge consisting of a triple bond linked to a methylene group. First, the two degrees of freedom, introduced by the sp^3-C, play a critical role on the individual chromophore optical properties as highlighted by quantum chemical calculations. Second, taking advantage of those freedom degrees and of the structure-directing pyridine group, chromophores are able to adopt conformations that lead to an unprecedented well-organization of the emitters into two-dimensional (2D) rectangular columnar-like supramolecular structure stabilized by intermolecular H-bonding. Finally, this result allows elucidating the origin for the yellow afterglow reported in the literature for carbazole-based derivatives as resulting from carbazole molecular columns. We have further shown that the formation of well-defined 2D columnar networks is favorable to reach long phosphorescence lifetimes, whereas intricate columns shorten them. Since our design approach appears quite general, our results give a new set of guidelines for the synthesis of long-lived organic phosphors.

Acknowledgements

This research was supported by the Asian Office of Aerospace Research and Development (AOARD, FA 2386-17-1-4060). We are very grateful to Prof. Ha-Jin Lee from the Korea Basic Science Institute (KBSI, Western Seoul Center) for the single crystal measurements. The authors thank the SYSPROD project and AXELERA Pkle de Comp8titivit8 for financial support (PSMN Data Center). J.W.W. acknowledges NRF grant (2017R1E1A1A01075394, 2014M3A6B3063708). A.J.A. and C.D. thank Dr. Jean-Louis Fave (INSP, Universit8 Sorbonne Universit8, Paris) for the very fruitful and friendly discussions.

Conflict of interest

The authors declare no conflict of interest.

Keywords: hydrogen bonds · molecular crystals · organic room-temperature phosphorescence · supramolecular self-assembly · s-conjugation

[1] R. Kabe, C. Adachi, *Nature* 2017, *550*, 384.
[2] S. Hirata, K. Totani, J. Zhang, T. Yamashita, H. Kaji, S. R. Marder, T. Watanabe, C. Adachi, *Adv. Funct. Mater.* 2013, *23*, 3386.
[3] S. Hirata, K. Totani, T. Yamashita, C. Adachi, M. Vacha, *Nat. Mater.* 2014, *13*, 938.
[4] S. Hirata, K. Totani, H. Kaji, M. Vacha, T. Watanabe, C. Adachi, *Adv. Opt. Mater.* 2013, *1*, 438.
[5] X.-F. Wang, H. Xiao, P.-Z. Chen, Q.-Z. Yang, B. Chen, C.-H. Tung, Y.-Z. Chen, L.-Z. Wu, *J. Am. Chem. Soc.* 2019, *141*, 5045.
[6] G. Zhang, G. M. Palmer, M. W. Dewhirst, C. L. Fraser, *Nat. Mater.* 2009, *8*, 747.
[7] J. Zhi, Q. Zhou, H. Shi, Z. An, W. Huang, *Chem. Asian J.* 2020, *15*, 947.
[8] Kenry, C. Chen, B. Liu, *Nat. Commun.* 2019, *10*, 1.
[9] Q. Li, Z. Li, *Adv. Sci.* 2017, *4*, 1600484.
[10] E. Hamzehpoor, D. F. Perepichka, *Angew. Chem. Int. Ed.* 2020, *59*, 9977; *Angew. Chem.* 2020, *132*, 10063.
[11] Y. Xie, Y. Ge, Q. Peng, C. Li, Q. Li, Z. Li, *Adv. Mater.* 2017, *29*, 1606829.
[12] W. Zhao, Z. He, J. W. Y. Lam, Q. Peng, H. Ma, Z. Shuai, G. Bai, J. Hao, B. Z. Tang, *Chem* 2016, *1*, 592.
[13] Y. Gong, G. Chen, Q. Peng, W. Z. Yuan, Y. Xie, S. Li, Y. Zhang, B. Z. Tang, *Adv. Mater.* 2015, *27*, 6195.
[14] Z. An, C. Zheng, Y. Tao, R. Chen, H. Shi, T. Chen, Z. Wang, H. Li, R. Deng, X. Liu, W. Huang, *Nat. Mater.* 2015, *14*, 685.
[15] J. Yang, X. Zhen, B. Wang, X. Gao, Z. Ren, J. Wang, Y. Xie, J. Li, Q. Peng, K. Pu, Z. Li, *Nat. Commun.* 2018, *9*, 1.
[16] W. Zhao, T. S. Cheung, N. Jiang, W. Huang, J. W. Y. Lam, X. Zhang, Z. He, B. Z. Tang, *Nat. Commun.* 2019, *10*, 1.
[17] L. Gu, H. Shi, L. Bian, M. Gu, K. Ling, X. Wang, H. Ma, S. Cai, W. Ning, L. Fu, H. Wang, S. Wang, Y. Gao, W. Yao, F. Huo, Y. Tao, Z. An, X. Liu, W. Huang, *Nat. Photonics* 2019, *13*, 406.
[18] Z. Yang, Z. Mao, X. Zhang, D. Ou, Y. Mu, Y. Zhang, C. Zhao, S. Liu, Z. Chi, J. Xu, Y.-C. Wu, P.-Y. Lu, A. Lien, M. R. Bryce, *Angew. Chem. Int. Ed.* 2016, *55*, 2181; *Angew. Chem.* 2016, *128*, 2221.
[19] Y. Xiong, Z. Zhao, W. Zhao, H. Ma, Q. Peng, Z. He, X. Zhang, Y. Chen, X. He, J. W. Y. Lam, B. Z. Tang, *Angew. Chem. Int. Ed.* 2018, *57*, 7997; *Angew. Chem.* 2018, *130*, 8129.

[20] F. Li, S. Guo, Y. Qin, Y. Shi, M. Han, Z. An, S. Liu, Q. Zhao, W. Huang, *Adv. Opt. Mater.* 2019, *7*, 1900511.
[21] D. J. Gibbons, A. Farawar, P. Mazzella, S. Leroy-Lhez, R. M. Williams, *Photochem. Photobiol. Sci.* 2020, *19*, 136.
[22] S. Hirata, Y. Sakai, K. Masui, H. Tanaka, S. Y. Lee, H. Nomura, N. Nakamura, M. Yasumatsu, H. Nakanotani, Q. Zhang, K. Shizu, H. Miyazaki, C. Adachi, *Nat. Mater.* 2015, *14*, 330.
[23] D.-H. Kim, A. D'Al8o, X.-K. Chen, A. D. S. Sandanayaka, D. Yao, L. Zhao, T. Komino, E. Zaborova, G. Canard, Y. Tsuchiya, E. Choi, J. W. Wu, F. Fages, J.-L. Br8das, J.-C. Ribierre, C. Adachi, *Nat. Photonics* 2018, *12*, 98.
[24] J. Gibson, A. P. Monkman, T. J. Penfold, *ChemPhysChem* 2016, *17*, 2956.
[25] B. Mettra, Y. Y. Liao, T. Gallavardin, C. Armagnat, D. Pitrat, P. Baldeck, T. L. Bahers, C. Monnereau, C. Andraud, *Phys. Chem. Chem. Phys.* 2018, *20*, 3768.
[26] G. F. Mes, B. De Jong, H. J. Van Ramesdonk, J. W. Verhoeven, J. M. Warman, M. P. De Haas, L. E. W. Horsman-Van den Dool, *J. Am. Chem. Soc.* 1984, *106*, 6524.
[27] A. M. Brouwer, N. A. C. Bakker, P. G. Wiering, J. W. Verhoeven, *J. Chem. Soc. Chem. Commun.* 1991, 1094.
[28] Y. Geng, A. D'Aleo, K. Inada, L.-S. Cui, J. U. Kim, H. Nakanotani, C. Adachi, *Angew. Chem. Int. Ed.* 2017, *56*, 16536; *Angew. Chem.* 2017, *129*, 16763.
[29] T. Le Bahers, C. Adamo, I. Ciofini, *J. Chem. Theory Comput.* 2011, *7*, 2498.
[30] C. Adamo, T. Le Bahers, M. Savarese, L. Wilbraham, G. Garcła, R. Fukuda, M. Ehara, N. Rega, I. Ciofini, *Coord. Chem. Rev.* 2015, *304 – 305*, 166.
[31] P. de Silva, C. A. Kim, T. Zhu, T. Van Voorhis, *Chem. Mater.* 2019, *31*, 6995.
[32] H. Ohkita, S. Ito, M. Yamamoto, Y. Tohda, K. Tani, *J. Phys. Chem. A* 2002, *106*, 2140.
[33] H. Benten, J. Guo, H. Ohkita, S. Ito, M. Yamamoto, N. Sakumoto, K. Hori, Y. Tohda, K. Tani, *J. Phys. Chem. B* 2007, *111*, 10905.
[34] C. S. Bilen, N. Harrison, D. J. Morantz, *Nature* 1978, *271*, 235.
[35] S. Cai, H. Shi, D. Tian, H. Ma, Z. Cheng, Q. Wu, M. Gu, L. Huang, Z. An, Q. Peng, W. Huang, *Adv. Funct. Mater.* 2018, *28*, 1705045.
[36] V. Jankus, A. P. Monkman, *Adv. Funct. Mater.* 2011, *21*, 3350.
[37] A. Marty, P. Viallet, *J. Photochem.* 1972, *1*, 443.
[38] H. Najafov, B. Lee, Q. Zhou, L. C. Feldman, V. Podzorov, *Nat. Mater.* 2010, *9*, 938.
[39] A. Kçhler, H. B-ssler, *J. Mater. Chem.* 2011, *21*, 4003.
[40] S. T. Hoffmann, P. Schrçgel, M. Rothmann, R. Q. Albuquerque, P. Strohriegl, A. Kçhler, *J. Phys. Chem. B* 2011, *115*, 414.